

Many-Body effects beyond excitons in second-harmonic generation of monolayer MoS₂

Peio Garcia-Goiricelaya¹, Julen Ibañez-Azpiroz^{2,3,4}

1 Department of Physics, University of the Basque Country UPV/EHU, 48940 Leioa, Basque Country, Spain

2 Centro de Física de Materiales, Universidad del País Vasco UPV/EHU, 20018 San Sebastián, Spain

3 Ikerbasque Foundation, 48013 Bilbao, Spain

* peio.garcia@ehu.eus, julen.ibanez@ehu.eus

February 27, 2026

Abstract

We present a quantitative study of many-body effects including the three-particle level on second-harmonic generation in monolayer MoS₂. Our approach combines many-body perturbation theory with time-dependent current-density-functional theory within an *ab initio* framework in the optical limit. Inclusion of two-particle excitonic effects *via* a dynamical long-range linear exchange–correlation kernel reproduces the qualitative features of the second-harmonic response, but underestimates the experimentally reported magnitudes by nearly a factor of two. By incorporating three-particle (trionic) correlations through a static long-range quadratic exchange-correlation kernel, we achieve significantly improved quantitative agreement with experiment. These findings highlight the role of many-body interactions beyond the excitonic level in accurately describing second-order optical responses in two-dimensional semiconductors.

Contents

1	Introduction	2
2	Computational details	4
3	Electronic band structure and linear optical response	5
4	Second harmonic generation: role of two-body and three-body effects	7
5	Conclusions and Outlook	10
A	Methodology	11
	A.1 Time-dependent density functional theory	11
	A.2 Time-dependent current-density functional theory	11
	A.3 TDCDFT in the optical and long-wavelength limit	12
	A.4 Macroscopic optical response	14
	References	14

1 Introduction

Nonlinear optics encompasses physical phenomena in which a material's response to incident light is not linearly proportional to the field amplitude [1]. Unlike the linear regime, nonlinear optical processes enable the generation of light at modified frequencies, for instance through second-harmonic generation (SHG) [2]. The last decade has witnessed a growing interest in higher-order optical responses for their technological potential. A notable example is the bulk photovoltaic effect that occurs in noncentrosymmetric crystals [3], investigated as a promising mechanism for direct current generation beyond conventional solar cells [4]. Similarly, nonlinear optical effects in topological materials have gained significant interest [5–9] due to their deep connection with topological Berry-phase-like quantities [10].

A robust and predictive theoretical understanding of nonlinear optics is therefore highly desirable for the development of emerging optical technologies [11]. In this context, first principles calculations based on density functional theory (DFT) play a central role, providing microscopic and system-specific insights [12–17]. However, achieving quantitative accuracy requires the explicit incorporation of many-body interactions into these theoretical frameworks [18]. This is particularly important in low-dimensional semiconducting systems, where reduced electronic screening amplifies many-body effects [19]. The emergence of many-particle correlated excitations often dominates the optical response of such nanostructured materials, which have rapidly become leading platforms for future technological applications [20].

A clear view of the role of many-body interactions in nonlinear optical responses can be obtained within the framework of time-dependent DFT (TDDFT) [21]. In this formalism, the quadratic density response function is expressed through a Dyson-like shorthand equation as [22]

$$\chi_{\rho 2} = \varepsilon^{-1} \chi_{\rho 2}^0 \varepsilon^{-1} \varepsilon^{-1} + \chi_{\rho 1} g_{xc} \chi_{\rho 1} \chi_{\rho 1}, \quad (1)$$

where the linear contribution is

$$\chi_{\rho 1} = \chi_{\rho 1}^0 \varepsilon^{-1}, \quad (2)$$

with $\varepsilon^{-1} = 1 + (v_c + f_{xc})\chi_{\rho 1}$ the inverse of the dielectric function and v_c the Coulomb interaction, *i.e.* the functional derivative of the Hartree potential. Above, $\chi_{\rho n}$ and $\chi_{\rho n}^0$ denote the many-body and independent-(quasi)particle density response functions at n -th order, respectively. In turn, f_{xc} and g_{xc} are the *unknown* linear and quadratic exchange-correlation (xc) kernels, *i.e.* the first and second functional derivatives of the exchange-correlation potential, respectively. As seen by the equations above, these terms drive the many-body renormalization of linear and quadratic optical responses and are therefore the primary focus of this study.

From a many-body perturbation theory (MBPT) perspective, Eqs. (2) and (1) are formally equivalent to the contraction of the correlation parts of the two- and three-particle Green's functions, respectively [23]. Importantly, this establishes a correspondence between the two- and three-body interactions and the linear f_{xc} and quadratic g_{xc} exchange-correlation kernels of TDDFT, respectively. Thus, when evaluating the response to light, f_{xc} encapsulates electron-hole interactions, as schematically illustrated in Fig. 1(a), leading to the formation of two-particle bound states, or *excitons* [24, 25]. In turn, g_{xc} incorporates the electron-electron-hole and electron-hole-hole interactions depicted in Figs. 1(b) and (c), respectively. The associated composite quasiparticles, known as *trions* or charged excitons, are three-particle bound states that emerge from neutral excitons upon carrier doping [26, 27].

The most direct way of computing nonlinear optical responses beyond the independent-particle approximation is to evaluate the response functions explicitly in terms of many-

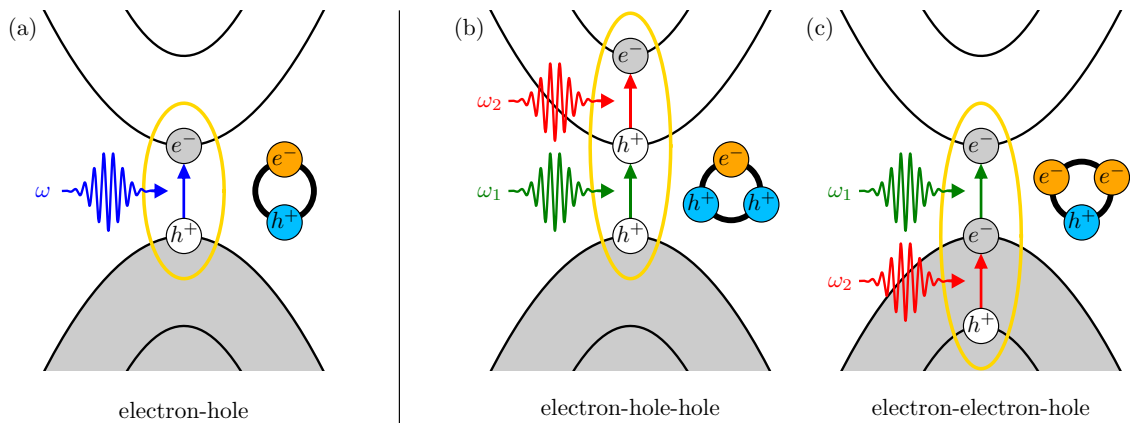


Figure 1: Schematic of two-particle (a) and three-particle (b,c) many-body interactions in the linear and quadratic optical response of a semiconductor, respectively. Grey and white shaded lines represent valence and conduction bands, respectively.

body wavefunctions and energies. Over the past two decades, such calculations have been extensively carried out at the two-particle level using a basis of excitonic states [28–42], while systematically neglecting trionic contributions. In parallel, state-of-the-art TDDFT approaches typically start from a quasiparticle-corrected non-interacting response and incorporate excitonic effects through long-range approximate forms of the linear exchange-correlation kernel, whereas quadratic effects are always omitted [43–48]. As evident from Eq. (1), this leads to a partially interacting second-order response that accounts only for two-particle correlations, again excluding three-particle contributions. This constitutes a significant limitation: just as the two-body electron-hole interaction is essential for describing linear optical absorption, nonlinear optical responses are likewise expected to be increasingly governed by many-body interactions beyond the two-particle level.

In this work, we investigate the influence of many-body interactions up to the three-particle level on SHG. We select monolayer MoS₂ as a case study for two main reasons. First, its reduced dimensionality gives rise to pronounced many-body excitonic [49–53] and trionic [54, 55] signatures in optical absorption and photoluminescence spectra. Second, this material, as well as similar transition-metal dichalcogenide compounds, have recently shown signatures of remarkable nonlinear optical processes [56–58]. These factors make monolayer MoS₂ an ideal testbed for our study. In addition, instead of TDDFT, we employ the framework of time-dependent current-density functional theory (TDCDFT) [59, 60] to compute the interacting many-body microscopic response. TDCDFT constitutes the tensor extension of TDDFT, in which the scalar charge density and electric potential are replaced by the vector current density and electric field, respectively, and scalar response functions by response tensors. Similarly, scalar exchange-correlation kernels are replaced by tensorial counterparts. We adopt the tensorial formulation of the response for several reasons. First, it provides a natural connection to the tensorial formulation of the response within the independent-particle picture in the optical limit. Second, it yields response equations that are free of long-wavelength divergences in the optical limit and of low-frequency divergences in the static limit. Third, it enables a direct macroscopic averaging of the microscopic response, which is ultimately the quantity accessible in experiment.

In a nutshell, our approach proceeds as follows. Single-particle excitations arising from the electron-electron interaction and two-particle excitations associated to the electron-hole interaction are taken into account within MBPT *via* the *GW* method and the Bethe-Salpeter equation (BSE), respectively. In this way, we obtain the macroscopic dielec-

tric response, which naturally incorporates quasiparticle corrections and excitonic effects. From this accurate description, we extract the long-range contribution of the two-body tensorial exchange–correlation kernel that reproduces the linear optical response. This kernel is then used in our state-of-the-art calculation of SHG, where we further assess the quantitative impact of the three-body tensorial exchange–correlation kernel associated with trionic effects. Our main result shows that including quadratic exchange–correlation contributions that account for trions leads to an improved quantitative agreement with experimental SHG spectra, emphasizing the important role of three-body interactions in accurately modeling second-order photoresponses.

The paper is organized as follows. In Sec. 2, we provide all the computational details of the calculations. The corresponding results are discussed in Secs. 3 and 4 for the linear and quadratic regimes, respectively. We conclude in Sec. 5 with a summary and discussion, and in Appendix A we describe our theoretical methodology.

2 Computational details

We performed ground-state electronic structure calculations using density functional theory (DFT) [61, 62] in the local density approximation (LDA) [63] as implemented in the QUANTUM ESPRESSO code package [64–66]. The interaction between valence electrons and atomic cores was modeled by means of norm-conserving pseudopotentials [67, 68] from the optimized norm-conserving Vanderbilt (ONCV) SG15 pseudopotentials database [69, 70] including fully relativistic corrections [71]. In the case of molybdenum, besides $4d$ and $5s$ valence electrons, $4s$ and $4p$ semi-core electrons were also explicitly included as valence states, since they are known to be crucial for proper self-energy calculations based on the GW method [50, 72]. Self-consistent DFT calculations were carried out using a \mathbf{k} -point mesh of 12×12 in combination with fixed occupation values and a plane-wave basis set with a cutoff energy of 100 Ry.

To model monolayer MoS₂, we considered a supercell (sc) with a hexagonal close-packed structure of two planes of sulfur atoms with an intercalated plane of molybdenum atoms. The in-plane lattice parameter is set equal to the experimental bulk value, *i.e.*, 3.16 Å [73], and a size of $L_{\text{sc}} = 20$ Å is set in the out-of-plane direction, providing a sufficiently large vacuum region in order to avoid spurious interactions between periodically repeated slabs. This is also enforced by the truncation of the Coulomb interaction following Ref. [74]. The equilibrium atomic positions were determined by relaxing all atomic forces up to at least 10^{-6} Ry/ a_0 , leading to a relaxed interplanar distance equal to 1.55 Å, equivalent to a Mo-S bond length of 2.39 Å, in good agreement with previous theoretical calculations [75, 76].

Starting from LDA wave functions and energies, we calculated quasiparticle (QP) corrections due to electron-electron interactions within the one-shot G_0W_0 approximation [77, 78] and, subsequently, linear optical absorption spectra including excitonic effects through BSE [79], as implemented in the YAMBO code package [80, 81]. Concerning G_0W_0 calculations, we selected the main parameters by focusing on the convergence of the QP band-gap energy, as well as the conduction-band minimum and valence-band maximum, with a threshold below 15 meV. We applied the plasmon-pole approximation [82–84] with an energy cutoff of 12 Ry and 40 Ry for the dielectric matrix and both the exchange and correlation parts of the self-energy, respectively, and we included up to 220 bands in the sum-over-states of the dielectric matrix and the correlation part of the self-energy. We obtained converged values for a \mathbf{k} -point mesh of 30×30 . To speed up the convergence with respect to empty states, we adopted the technique described in Ref. [85]. In addition,

to accelerate convergences with respect to the \mathbf{k} -point sampling avoiding long-wavelength divergences of the electronic potential, we used the so-called random integration method of the screened potential (RIM-W) [86] together with the truncation of the Coulomb potential in the slab geometry. In this way, we performed Monte Carlo integrations with 2×10^6 random points taking into account \mathbf{G} vectors up to 2.5 Ry and 1 Ry for the bare and screened Coulomb potentials, respectively. For the BSE calculations, we employed the Lanczos-Haydock solver [87], since our interest lies in the excitonic optical spectrum rather than in storing the full excitonic wave functions. An energy cutoff of 25 Ry and 8 Ry is used for the electron-hole exchange and attraction parts, respectively, of the BSE kernel, and 14 occupied and 22 unoccupied states have been used to build up the excitonic Hamiltonian. We used a \mathbf{k} -point mesh of 33×33 , which is enough to provide a good convergence in the position of the excitonic peaks.

As a next step, we evaluated non-interacting SHG susceptibility tensors at LDA and G_0W_0 levels in the optical and long-wavelength limit. We considered the length-gauge expressions [88–91] as implemented in the WANNIER90 code package [48, 92]. To this end, starting from a set of 48 spin-split bands, we constructed 36 disentangled maximally localized Wannier functions (MLWFs) spanning the 14 high-energy valence bands and the 22 low-energy conduction bands using two p trial orbitals centered on S atoms, as well as one s and one d trial orbitals centered on the Mo atom. To obtain well-converged optical spectra, we used a dense \mathbf{k} -point interpolated mesh of 1000×1000 . With respect to the imaginary part of the complex $\hbar\omega$, we set $\eta = 0.1$ eV, consistent with photoexcited carrier lifetimes (~ 10 fs) [93]. Regarding the auxiliary parameter for regularizing energy denominators, we chose $\eta_r = 0.05$ eV. The occupation factors and their derivatives were evaluated at zero temperature ($T = 0$ K).

Following a well-established procedure [91], we rescaled the response tensors by the factor $L_{\text{sc}}/L_{\text{eff}}$, where L_{eff} accounts for the effective thickness of the monolayer and L_{sc} is the size of the supercell described earlier. In this way, the effective macroscopic dielectric tensor reads as $\epsilon_{\text{M}}(\omega) = \mathbb{1} + \chi_1(\omega)L_{\text{sc}}/L_{\text{eff}}$ [94], where $\chi_1(\omega)$ represents the macroscopic linear susceptibility tensor of the supercell and ω the frequency dependence. We used a value of $L_{\text{eff}} = 7.3$ Å, which we have obtained considering the spatial extent of the charge density along the out-of-plane direction, as visualized in Fig. 2(a). This value aligns closely with the experimental atomic thickness of approximately 8 Å reported in the Supplemental Information of Ref. [56]. We note that the effective thickness we employ differs from the value assumed in other works $L_{c/2} = 6.15$ Å, which corresponds to half of the out-of-plane bulk lattice parameter [73] [see Fig. 2(a)].

3 Electronic band structure and linear optical response

We begin by inspecting the electronic band structure of monolayer MoS₂. The LDA calculation shown by solid grey lines in Fig. 2(b) predicts that the system is a semiconductor with a direct energy band gap of about 1.65 eV at high symmetry point \bar{K} . In order to improve this description, we include quasiparticle corrections to the band structure by approximating self-energy effects of single-particle excitations arising from the electron–electron interaction within the one-shot G_0W_0 approximation. The resulting quasiparticle band dispersion is illustrated by the dashed red lines in Fig. 2(b), which predicts a direct band gap of 2.52 eV.

We next focus on the linear optical response. In order to capture excitonic effects of two-particle excitations arising from the electron-hole interaction, we solve BSE to obtain the macroscopic optical dielectric spectrum. In Fig. 3(a), we compare this quantity as

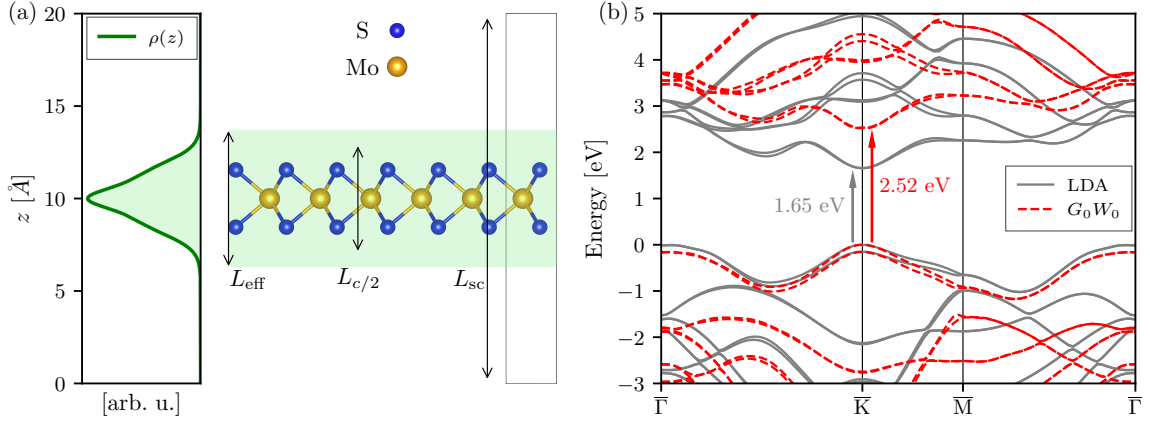


Figure 2: (a) Out-of-plane extension of the in-plane averaged charge density (left) together with the OYZ side view of the slab crystal unit (right) of monolayer MoS_2 . Supercell thickness, effective thickness, and half of the bulk thickness are $L_{sc} = 20$ Å, $L_{eff} = 7.3$ Å and $L_{c/2} = 6.15$ Å [73], respectively. The green-shaded area highlights the effective out-of-plane spatial extent of the electrons. (b) LDA (solid grey lines) and G_0W_0 (dashed red lines) electronic band structure of monolayer MoS_2 . LDA and G_0W_0 direct energy band gaps are equal to 1.65 eV and 2.52 eV, respectively.

calculated within the G_0W_0 and BSE approaches, shown by the narrow red and broad blue lines, respectively. The BSE results exhibit very good agreement with experimental data [95], shown by yellow lines with circles, and clearly improved upon the G_0W_0 spectrum by incorporating two-body excitonic effects. Indeed, the BSE optical spectrum captures the spin-split A and B exciton double-peak structure between 2 and 2.15 eV, followed by the C peak around 2.7 eV. All these results are in good agreement with previous DFT plus MBPT calculations [49–53].

Based on the BSE results shown in Fig. 3(a), we now proceed to construct a tensorial exchange-correlation kernel in the linear regime that accounts for excitonic effects within TDCDFT. In the optical limit, the linear exchange-correlation kernel of TDDFT is dominated by its long-range contribution (LRC) and behaves *exactly* like an attractive screened Coulomb interaction that emulates the electron-hole attraction, in such a way that $\lim_{\mathbf{q} \rightarrow 0} f_{xc}(\mathbf{q}) = -\alpha_{\text{LRC}}/q^2$, where \mathbf{q} is the crystal momentum transfer and the screening parameter α_{LRC} is an *unknown* material-dependent quantity [96, 97]. Empirical [98–100] and nonempirical [101–107] static evaluations of the linear LRC screening parameter have only proven to work well to some extent for *continuum* excitonic effects and at most one bound exciton peak, but fail to describe multiple excitonic features. On the other hand, a dynamical extension of this quantity has been shown to be essential in order to reproduce subtle excitonic features within TDDFT starting from very good evaluations of the macroscopic optical dielectric function that can be, for instance, the result of BSE [108, 109].

As for TDDFT, one can derive an expression for calculating the linear LRC screening tensor within TDCDFT in the optical limit, in such a way that

$$\alpha_{\text{LRC}}(\omega) = -4\pi \left\{ [\epsilon_{\text{BSE}}(\omega) - 1]^{-1} - [\epsilon_{\text{RPA}}(\omega) - 1]^{-1} \right\}, \quad (3)$$

where $\epsilon_{\text{RPA}}(\omega)$ denotes the optical dielectric tensor in the random phase approximation (RPA), *i.e.* neglecting many-body interactions, and $\epsilon_{\text{BSE}}(\omega)$ the BSE optical dielectric tensor including excitonic effects.

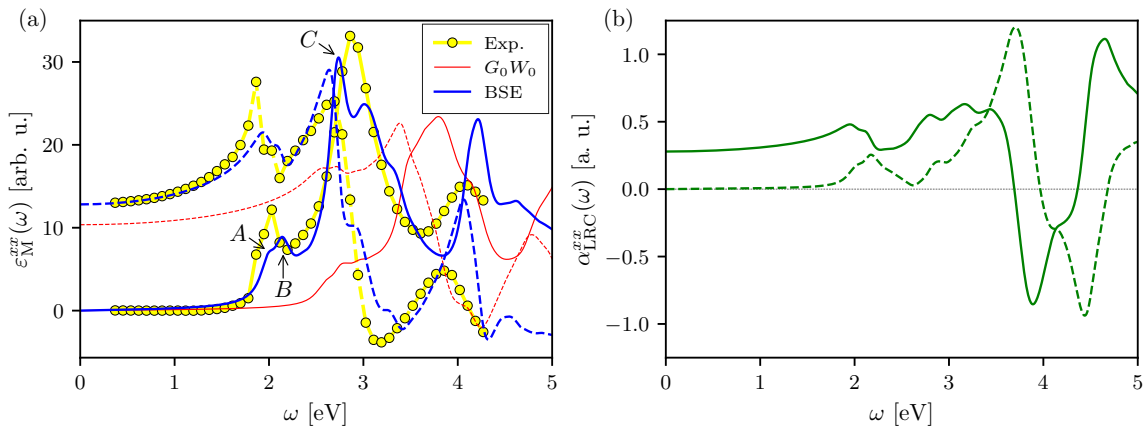


Figure 3: (a) Macroscopic optical dielectric spectrum of MoS₂. Dashed and solid yellow lines with circles represent the real and imaginary parts of experimental data, respectively, from Ref. [95]. Dashed and solid narrow red (broad blue) lines represent the real and imaginary parts within the G_0W_0 (BSE) picture, respectively. (b) In-plane longitudinal component of the linear LRC screening tensor $\alpha_{\text{LRC}}^{xx}(\omega)$. Solid and dashed green lines represent the real and imaginary parts, respectively.

The in-plane longitudinal component of the linear LRC screening tensor calculated in this way is shown in Fig. 3(b). The figure shows a rather intricate structure, with multiple peaks and dips in both the real and imaginary parts of $\alpha_{\text{LRC}}(\omega)$ in the excitonic frequency region. Importantly, this fine structure going beyond what can be achieved by simple approaches allows to incorporate the multippeak structure of excitons into TDCDFT.

An approximate analytic form of the dynamical linear exchange-correlation kernel, constructed from the Lorentz oscillator model that mimics poles extracted from experimentally measured optical absorption spectra, appears to recover more of these spectral features and is therefore particularly appealing for an alternative practical implementation [110].

4 Second harmonic generation: role of two-body and three-body effects

We are now in a position to address our central objective of calculating the macroscopic second harmonic susceptibility from first principles. This is achieved by performing the macroscopic averaging of the microscopic SHG polarizability [45], whose interacting form can be calculated using the tensorial expression derived in Ref. [48] within TDCDFT. The adaptation of these response equations in the optical limit, including three-body interactions, appears in Appendix A. For this formulation, we exploit the *exact* static behavior of the quadratic exchange-correlation kernel of TDDFT in the optical limit, which has been derived from a second-order BSE for the three-particle correlation function [23]. In this limit, the long-range contribution dominates, such that $\lim_{\mathbf{q} \rightarrow 0} g_{\text{xc}}(\mathbf{q}, \mathbf{q}) = \beta_{\text{LRC}}/q^3$ [23], where β_{LRC} is a material-dependent parameter. In this way, the microscopic SHG polarizability tensor is expressed through a Dyson-like equation as

$$\begin{aligned} \alpha_2(\omega, \omega) = & \varepsilon^{-1,T}(2\omega) \alpha_2^0(\omega, \omega) \varepsilon^{-1}(\omega) \varepsilon^{-1}(\omega) \\ & + i \alpha_1^T(2\omega) \beta_{\text{LRC}}(\omega, \omega) \alpha_1(\omega) \alpha_1(\omega), \end{aligned} \quad (4)$$

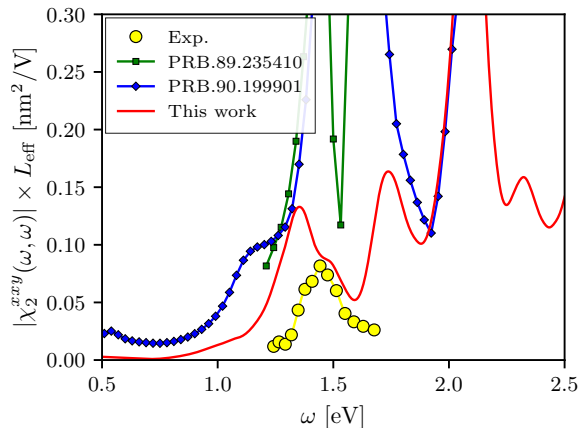


Figure 4: Absolute value of the macroscopic two-dimensional SHG susceptibility per unit area of monolayer MoS₂. The yellow line with circles dots represents experimental data from Ref. [56]. Blue lines with diamonds and green lines with squares represent theoretical results including excitonic effects from Refs. [30, 31] and [32], respectively. Red lines represent our theoretical results including excitonic effects.

where the microscopic linear optical polarizability tensor reads as $\alpha_1(\omega) = \alpha_1^0(\omega)\epsilon^{-1}(\omega)$ with $\epsilon^{-1}(\omega) = \mathbb{1} - [4\pi - \alpha_{\text{LRC}}(\omega)]\alpha_1(\omega)$ the inverse of the optical dielectric tensor. In Eq. (4), two-body excitonic effects enter through the optical dielectric tensor, with $\alpha_{\text{LRC}}(\omega)$ extracted from BSE, as shown in Fig. 3(b). In turn, three-body trionic effects are incorporated *via* β_{LRC} .

Unlike conventional (first-order) BSE, its second-order counterpart has not yet been implemented in practical calculations; therefore, the tensor β_{LRC} cannot be obtained in the same way as α_{LRC} . As a result, no previous studies appear to have addressed its explicit evaluation. Nevertheless, by comparing experimental spectra with theoretical results that include many-body effects only up to the two-particle level, a reasonable range of values for β_{LRC} can be inferred, as we do next.

Guided by this objective, we evaluate the response by gradually turning on many-body interactions. In Fig. 4, we compare the calculated absolute value of the macroscopic SHG susceptibility, including only excitonic effects at the two-particle level, with other theoretical results obtained at the same level of many-body interactions [30–32], as well as with the available experimental data [56]. The onset of the SHG signal occurs around 1 eV, coinciding with half the eigenvalues of spin-split *A* and *B* bound excitons [see Fig. 3(a)]. The signal then reaches its first pronounced maximum through the strongly absorbing bound exciton *C* [see Fig. 3(a)], as half of its eigenvalue coincides with the energy of the corresponding SHG peak (see Fig. 4). Accordingly, our calculations predict a well-defined SHG resonance at 1.35 eV, in very good agreement with experiment, which shows an SHG peak at slightly below 1.5 eV. Although previous theoretical works have captured this overall trend [30–32], our results additionally exhibit remarkable quantitative agreement in intensity. In contrast, earlier studies required an empirical rescaling of their spectra to reproduce the experimental magnitude of the SHG response. This improvement arises from two main factors. First, Wannier interpolation allows for Brillouin zone sampling several orders of magnitude denser than those employed in previous works, significantly enhancing numerical convergence and accuracy. Second, we have adopted an effective layer thickness determined from the spatial extent of the charge density along the out-of-plane direction of the supercell, rather than the conventional choice of one half of the bulk

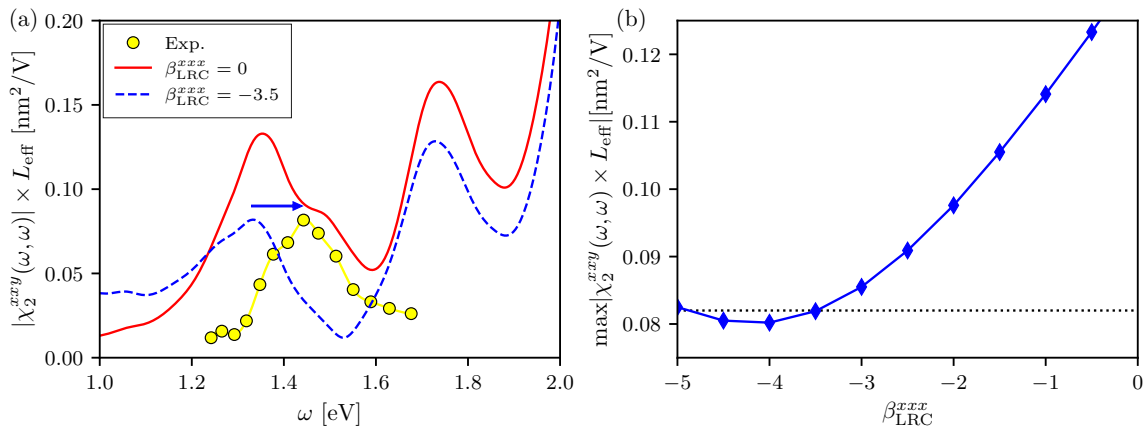


Figure 5: (a) Absolute value of the macroscopic two-dimensional SHG susceptibility per unit area of monolayer MoS₂. Yellow dots represent experimental data from Ref. [56]. Red lines represent our theoretical results including many-body interactions up to the two-particle level, *i.e.* excitonic effects, while dashed blue line includes also at the three-particle level, *i.e.* trionic effects. (b) Theoretical value of the height of the peak close to 1.5 eV as a function of the in-plane longitudinal component of the quadratic LRC β_{LRC} tensor of the quadratic exchange-correlation kernel with the dotted line being the experimental value.

lattice constant. This definition is consistent with the experimentally measured atomic thickness [56] and provides a more physically grounded estimate.

Despite the substantial improvement over previous theoretical predictions, our SHG result still yields an intensity of approximately $0.14 \text{ nm}^2/\text{V}$, significantly above the experimental value of $0.08 \text{ nm}^2/\text{V}$. At this stage, our treatment accounts for many-body interactions only up to the two-particle level, meaning that only the first term on the r.h.s. of Eq. (4) has been considered in the evaluation of the microscopic SHG response. However, it is the second term that accounts for many-body effects at the three-particle level, which are themselves linearly screened, as the tensor β_{LRC} correlates three interacting linear responses. Therefore, it is reasonable to expect that if an effect is large at first order, it will also manifest prominently at second order. This idea contradicts the common approximation in the literature of disregarding the quadratic exchange-correlation kernel [43–48].

As far as we know, this work represents the first attempt to analyze three-particle many-body effects on quadratic optical responses, and, therefore, to assess the complete many-body response up to second order. In order to find an adequate value of the unknown quadratic LRC parameter, we compare the maximum SHG peak intensity from our theoretical predictions with the experimental value as a function of the in-plane longitudinal component of β_{LRC} [see Fig. 5(b)]. We find that a value of $\beta_{\text{LRC}}^{xxx} = -3.5$ a. u. reproduces the experimental peak intensity. The corresponding SHG spectrum is shown alongside experimental measurements in Fig. 5(a). Besides the maximum response value, the shape of the main SHG peak at 1.4 eV is very well captured by our calculations, with only a ~ 0.1 eV energy redshift of our computed result compared to experiment, a discrepancy that lies within the typical uncertainty of *GW* and *BSE* calculations within the MBPT framework.

5 Conclusions and Outlook

In summary, our *ab initio* results demonstrate that many-body interactions beyond the two-particle level are necessary for a quantitative description of the SHG spectrum in monolayer MoS₂. By incorporating trionic bound-state contributions through a static long-range quadratic exchange–correlation kernel, we obtain close agreement with experiment in both peak positions and intensities. These findings reveal that three-body effects –almost universally neglected in standard theoretical treatments– can play a decisive role in second-order optical processes. More broadly, our work closes a quantitative gap between theory and experiment for SHG in low-dimensional semiconductors and establishes a framework for improved predictions of other quadratic optical responses in emerging nanomaterials.

Following the present analysis for SHG, it becomes interesting to inspect the effect of three-particle interactions in the shift- and injection-current contributions to BPVE [3]. Such quadratic optical processes occur when the absorbed two photons have opposite energies, *i.e.* $\omega_1 = \omega = -\omega_2$ [see Figs. 1(b,c)]. In this scenario, the electron, which is previously excited to the conduction band by absorbing one photon of frequency ω , is then relaxed to the valence band by absorbing a second photon of frequency $-\omega$. During this process, the photoexcited carrier travels a finite distance or acquires a finite velocity in the real space, leading to the shift and injection currents, respectively. This is due to the lack of inversion symmetry, inherent to any second-order optical response. Adapting Eq. A18 from Appendix A, the Dyson-like expression in the frequency domain that accounts for such interacting optical conductivity tensors at the microscopic level within TDCDFE reads as [48]

$$\begin{aligned} \sigma_2(\omega, -\omega) = & \varepsilon^{-1T}(0) \sigma_2^0(\omega, -\omega) \varepsilon^{-1}(\omega) \varepsilon^{-1}(-\omega) \\ & + i \sigma_1^T(0) \frac{\beta_{\text{LRC}}(\omega, -\omega)}{\omega^2} \sigma_1(\omega) \sigma_1(-\omega), \end{aligned} \quad (5)$$

where σ_n and σ_n^0 are the interacting and non-interacting conductivity tensors at n -th order. By inspecting Eq. 5, we note that in technologically promising semiconductors with a finite band gap, the first term on the r.h.s. can be non zero, whereas the second term will always vanish. This follows from the fact that, in undoped semiconductors, the lineal conductivity in the static limit is zero, that is, $\sigma_1(0) = 0$. As a result, when analyzing the shift- and injection-current contributions to BPVE, many-body effects enter only by means of the first term, thus limited to the two-particle excitonic level. In this manner, previous calculations based on excitonic wavefunctions and eigenvalues can be considered formally correct in accounting of many-body interactions [36, 37, 39–42].

Acknowledgements

The authors are grateful to Alejandro Molina-Sánchez for helpful discussions related with GW & BSE calculations as well as guidance using the YAMBO code. The authors acknowledge financial support of the European Union’s Horizon 2020 research and innovation programme under the European Research Council (ERC) grant agreement No. 946629. J. I.-A. also acknowledges financial support of the Spanish Ministry of Science, Innovation and Universities (MICIU) under the “Proyectos de Generación de Conocimiento” grant No. PID2023-147324NA-I00.

A Methodology

In this unique appendix, we review the main derivation steps for obtaining handable microscopic response equations within TDCDFT in the optical limit starting from TDDFT. Finally, the macroscopic-microscopic connection of the response is also mentioned.

A.1 Time-dependent density functional theory

In TDDFT, one investigates the density response of a many-body system of electrons interacting *via* the Coulomb interaction to an externally applied time-dependent potential. Alternatively, one can adopt the auxiliary Kohn-Sham system of independent and non-interacting electrons, where the density response is now viewed with respect to the total time-dependent potential felt by the particles. For quadratic responses, this entails expanding the time-dependent density response of the interacting system in a power series of the external potential up to second order,

$$\rho(1) = \int_0^1 \chi_1(1, 2) V_{\text{ext}}(2) d2 + \iint_0^1 \chi_2(1, 2, 3) V_{\text{ext}}(2) V_{\text{ext}}(3) d2d3, \quad (\text{A1})$$

or, in the non-interacting case, in a power series of the total potential,

$$\rho(1) = \int_0^1 \chi_1^0(1, 2) V_{\text{tot}}(2) d2 + \iint_0^1 \chi_2^0(1, 2, 3) V_{\text{tot}}(2) V_{\text{tot}}(3) d2d3, \quad (\text{A2})$$

where we adopted the notation $(\mathbf{r}_n, t_n) \equiv (n)$ with n a positive integer and with the total potential related to the external potential as

$$V_{\text{tot}}(\mathbf{r}, t) = V_{\text{ext}}(\mathbf{r}, t) + V_{\text{H}}(\mathbf{r}, t) + V_{\text{xc}}(\mathbf{r}, t). \quad (\text{A3})$$

The Hartree potential as a function of the density response is given by

$$V_{\text{H}}(1) = \int_0^1 v_c(1, 2) \rho(2) d2, \quad (\text{A4})$$

with the Coulomb interaction $v_c(1, 2) = \delta(t_1 - t_2)/|\mathbf{r}_1 - \mathbf{r}_2|$, and the exchange-correlation potential up to second order is written as

$$V_{\text{xc}}(1) = \int_0^1 f_{\text{xc}}(1, 2) \rho(2) d2 + \iint_0^1 g_{\text{xc}}(1, 2, 3) \rho(2) \rho(3) d2d3. \quad (\text{A5})$$

Applying now the chain rule in the definition of the many-body density response functions and taking into account the definition of the independent-particle density response function as well as the relation between the total and external potentials, one arrives to Eqs. 2 and 1 at first and second order, respectively.

A.2 Time-dependent current-density functional theory

TDCDFT follows the same basics as TDDFT, but the difference is that we are now interested in the microscopic response of the current-density to an externally applied time-dependent electric field, in the case of the many-body system, or to the total time-dependent electric field, in the case of the independent-particle system. From the mathematical point of view, this change of paradigm means that we are no longer interested

in scalar quantities, but in vectors and tensors. In this way, up to second order, the time-dependent current-density response can be written as

$$\mathbf{j}(1) = \int_0^1 \boldsymbol{\sigma}_1(1, 2) \mathbf{E}_{\text{ext}}(2) d2 + \int \int_0^1 \boldsymbol{\sigma}_2(1, 2, 3) \mathbf{E}_{\text{ext}}(2) \mathbf{E}_{\text{ext}}(3) d2 d3, \quad (\text{A6})$$

or alternatively as

$$\mathbf{j}(1) = \int_0^1 \boldsymbol{\sigma}_1^0(1, 2) \mathbf{E}_{\text{tot}}(2) d2 + \int \int_0^1 \boldsymbol{\sigma}_2^0(1, 2, 3) \mathbf{E}_{\text{tot}}(2) \mathbf{E}_{\text{tot}}(3) d2 d3, \quad (\text{A7})$$

where $\boldsymbol{\sigma}_n$ and $\boldsymbol{\sigma}_n^0$ are the interacting –many-body– and non-interacting –independent–(quasi)particle– current-density response tensors at n -th order, and the total electric field is related to the external electric field as

$$\mathbf{E}_{\text{tot}}(\mathbf{r}, t) = \mathbf{E}_{\text{ext}}(\mathbf{r}, t) + \mathbf{E}_{\text{H}}(\mathbf{r}, t) + \mathbf{E}_{\text{xc}}(\mathbf{r}, t). \quad (\text{A8})$$

The Hartree electric field as a function of the current-density response is given by

$$\mathbf{E}_{\text{H}}(1) = \int_0^1 \mathbf{K}_{\text{H}}(1, 2) \mathbf{j}(2) d2, \quad (\text{A9})$$

where \mathbf{K}_{H} is the tensorial Hartree kernel, which represents the tensor extension of the Coulomb interaction. In turn, the exchange-correlation electric field up to second order is written as

$$\mathbf{E}_{\text{xc}}(1) = \int_0^1 \mathbf{F}_{\text{xc}}(1, 2) \mathbf{j}(2) d2 + \int \int_0^1 \mathbf{G}_{\text{xc}}(1, 2, 3) \mathbf{j}(2) \mathbf{j}(3) d2 d3, \quad (\text{A10})$$

with \mathbf{F}_{xc} and \mathbf{G}_{xc} the linear and quadratic tensorial exchange-correlation kernels, respectively, which can also be viewed as the tensor extension of f_{xc} and g_{xc} .

As for the density response, applying the chain rule in the definition of the many-body current-density response tensors and taking into account the definition of the independent-particle current-density response tensors as well as the relation between the total and external electric fields, the Dyson-like linear and quadratic current-density response equations are derived,

$$\boldsymbol{\sigma}_1(1, 2) = \int \boldsymbol{\sigma}_1^0(1, 3) \boldsymbol{\varepsilon}^{-1}(3, 2) d3, \quad (\text{A11})$$

with $\boldsymbol{\varepsilon}^{-1}(1, 2) = \mathbf{1} + \int \mathbf{F}_{\text{xc}}(1, 3) \boldsymbol{\sigma}(3, 2) d3$ the inverse of the dielectric tensor, and

$$\begin{aligned} \boldsymbol{\sigma}_2(1, 2, 3) = \int \int \int & [\boldsymbol{\varepsilon}^{-1, T}(1, 4) \boldsymbol{\sigma}_2^0(4, 5, 6) \boldsymbol{\varepsilon}^{-1}(5, 2) \boldsymbol{\varepsilon}^{-1}(6, 3) \\ & + \boldsymbol{\sigma}_1^T(1, 4) \mathbf{G}_{\text{xc}}(4, 5, 6) \boldsymbol{\sigma}_1(5, 2) \boldsymbol{\sigma}_1(6, 3)] d4 d5 d6, \end{aligned} \quad (\text{A12})$$

respectively. As can be seen directly, Eqs. A11 and A12 are nothing but the tensor extension of Eqs. 2 and 1.

A.3 TDCDFT in the optical and long-wavelength limit

Since we are interested in optical responses, it is convenient to adapt TDCDFT equations to the optical and long-wavelength limit, which assumes that the microscopic response remains constant in the length-scale of the crystal's unit cell.

Regarding the Hartree contribution, the TDDFT Hartree potential is defined in Eq. A4, while the TDCDFT Hartree electric field is defined by Eq. A9. With the aid of Maxwell's equation $\mathbf{E}(\mathbf{r}, t) = -\nabla V(\mathbf{r}, t)$ and the continuity equation $\nabla \cdot \mathbf{j}(\mathbf{r}, t) = -\partial_t \rho(\mathbf{r}, t)$, one can

reformulate the TDCDFT Hartree electric field in the wave-vector and frequency space starting from the TDDFT Hartree potential and compare it with its original definition. In this way, the tensorial Hartree kernel can be expressed as

$$\mathbf{K}_H(\mathbf{q}_1, \mathbf{q}_2, \omega) = \frac{4\pi}{i\omega} \delta_{\mathbf{q}_1 \mathbf{q}_2} \frac{\mathbf{q}_1 \odot \mathbf{q}_2}{|\mathbf{q}_1||\mathbf{q}_2|}, \quad (\text{A13})$$

where \mathbf{q}_n represents the crystal momentum transfer of the n -th particle. In the optical limit, *i.e.* $\lim_{\mathbf{q}_n \rightarrow 0}$, the tensorial Hartree kernel reads then

$$\mathbf{K}_H(\omega) = \frac{4\pi}{i\omega} \mathbb{1}. \quad (\text{A14})$$

With respect to the exchange-correlation terms, we assume that the nonlocal long-range contribution (LRC) dominates over all other terms in the optical limit. In this way, excitonic and trionic effects in the optical limit within TDDFT are included by means of *exact* behaviors of the linear and quadratic xc kernels $\lim_{\mathbf{q}_n \rightarrow 0} f_{xc}(\mathbf{q}_1, \mathbf{q}_2, \omega) = -\alpha_{\text{LRC}}/q^2$ [96] and $\lim_{\mathbf{q}_n} g_{xc}(\mathbf{q}_1, \mathbf{q}_2, \mathbf{q}_3, \omega_1, \omega_2) = \beta_{\text{LRC}}/q^3$ [23], respectively. Both limits are derived from the first-order BSE two-particle and second-order BSE three-particle correlation functions within MBPT, respectively. Following the same procedure used for the optical tensorial Hartree kernel, we also derive the expressions of the linear and quadratic tensorial exchange-correlation kernels in the optical limit, which reads as

$$\mathbf{F}_{xc}(\omega) = \frac{-\alpha_{\text{LRC}}}{i\omega}, \quad (\text{A15})$$

and

$$\mathbf{G}_{xc}(\omega_1, \omega_2) = \frac{\beta_{\text{LRC}}}{i\omega_1\omega_2}, \quad (\text{A16})$$

respectively. α_{LRC} and β_{LRC} are second and third-rank diagonal tensors due to the longitudinal nature of long-range interactions in the optical limit. Thus, taking into account these definitions, one can already write the Dyson-like linear and quadratic current-density response equations in the optical limit as

$$\boldsymbol{\sigma}_1(\omega) = \boldsymbol{\sigma}_1^0(\omega) \boldsymbol{\varepsilon}^{-1}(\omega), \quad (\text{A17})$$

with $\boldsymbol{\varepsilon}^{-1}(\omega) = \mathbb{1} + \frac{4\pi - \alpha_{\text{LRC}}}{i\omega} \boldsymbol{\sigma}_1(\omega)$ the inverse of the optical dielectric tensor, and

$$\begin{aligned} \boldsymbol{\sigma}_2(\omega_1, \omega_2) = & \boldsymbol{\varepsilon}^{-1,T}(\omega_1 + \omega_2) \boldsymbol{\sigma}_2^0(\omega_1, \omega_2) \boldsymbol{\varepsilon}^{-1}(\omega_1) \boldsymbol{\varepsilon}^{-1}(\omega_2) \\ & + \boldsymbol{\sigma}_1^T(\omega_1 + \omega_2) \frac{\beta(\omega_1, \omega_2)}{i\omega_1\omega_2} \boldsymbol{\sigma}_1(\omega_1) \boldsymbol{\sigma}_1(\omega_2) \quad , \end{aligned} \quad (\text{A18})$$

respectively. Here, the advantage of using TDCDFT in the optical limit becomes evident, as one obtains current-density response equations that are independent of the wave vector, in contrast to the divergences that arise in density-based response functions within TDDFT in the optical limit. Nevertheless, divergences related to the frequency are still present. These are especially cumbersome for semiconductors, which present zero conductivity as the frequency goes to zero, leading to an indeterminate form of 0/0.

In this case, the response equations can be reformulated as a function of the polarization density instead of the current density. The optical polarization-density response with respect to the many-body system and to the independent-particle system is described as

$$\mathbf{p}(\omega = \omega_1 + \omega_2) = \boldsymbol{\alpha}_1(\omega) \mathbf{E}_{\text{ext}}(\omega) + \boldsymbol{\alpha}_2(\omega_1, \omega_2) \mathbf{E}_{\text{ext}}(\omega_1) \mathbf{E}_{\text{ext}}(\omega_2), \quad (\text{A19})$$

and

$$\mathbf{p}(\omega = \omega_1 + \omega_2) = \boldsymbol{\alpha}_1^0(\omega) \mathbf{E}_{\text{tot}}(\omega) + \boldsymbol{\alpha}_2^0(\omega_1, \omega_2) \mathbf{E}_{\text{tot}}(\omega_1) \mathbf{E}_{\text{tot}}(\omega_2), \quad (\text{A20})$$

respectively, where α_n and α_n^0 are the interacting –many-body– and non-interacting –independent-(quasi)particle– polarizability tensors at n -th order, respectively. In the absence of magnetization and free charge and current densities, the current and polarization-density vectors are related by $\mathbf{j}(\mathbf{r}, t) = \partial_t \mathbf{p}(\mathbf{r}, t)$. This implies that conductivity and polarizability tensors in the frequency domain are related in such a way that $\sigma_1^{(0)}(\omega) = -i\omega\alpha_1^{(0)}(\omega)$ and $\sigma_2^{(0)}(\omega_1, \omega_2) = -i(\omega_1 + \omega_2)\alpha_2^{(0)}(\omega_1, \omega_2)$ at first and second order, respectively. Making the pertinent substitutions, we finally write the Dyson-like linear and quadratic optical polarization-density response equations as

$$\alpha_1(\omega) = \alpha_1^0(\omega)\epsilon^{-1}(\omega), \quad (\text{A21})$$

with $\epsilon^{-1}(\omega) = \mathbb{1} - [4\pi - \alpha_{\text{LRC}}]\alpha_1(\omega)$ the inverse of the optical dielectric tensor, and

$$\begin{aligned} \alpha_2(\omega_1, \omega_2) = & \epsilon^{-1,T}(\omega_1 + \omega_2)\alpha_2^0(\omega_1, \omega_2)\epsilon^{-1}(\omega_1)\epsilon^{-1}(\omega_2) \\ & + i\alpha_1^T(\omega_1 + \omega_2)\beta(\omega_1, \omega_2)\alpha_1(\omega_1)\alpha_1(\omega_2) \end{aligned}, \quad (\text{A22})$$

respectively, free of any kind of divergence as can be seen. Hence, these are the equations we use in this work in order to account for many-body effects within the optical response up to second order at the microscopic level.

A.4 Macroscopic optical response

The ultimate goal of this work is thus to calculate the macroscopic optical susceptibility tensor from first principles and compare it with experiment. This is done by performing a macroscopic average of the microscopic optical polarizability tensor given by Eqs. A21 and A22 [48]. In atomic units, this task is done by means of the following expressions for first and second order,

$$\chi_1(\omega) = 4\pi\alpha_1(\omega)\epsilon_{\text{M}}(\omega) \quad (\text{A23})$$

and

$$\chi_2(\omega_1, \omega_2) = 4\pi\epsilon_{\text{M}}(\omega_1 + \omega_2)\alpha_2(\omega_1, \omega_2)\epsilon_{\text{M}}(\omega_1)\epsilon_{\text{M}}(\omega_2), \quad (\text{A24})$$

respectively, where the macroscopic optical dielectric tensor is given by

$$\epsilon_{\text{M}}(\omega) = [\mathbb{1} - 4\pi\alpha_1(\omega)]^{-1}. \quad (\text{A25})$$

References

- [1] R. Boyd and D. Prato, *Nonlinear Optics*, Elsevier Science, ISBN 9780080485966 (2008).
- [2] P. A. Franken, A. E. Hill, C. W. Peters and G. Weinreich, *Generation of optical harmonics*, Phys. Rev. Lett. **7**, 118 (1961), doi:10.1103/PhysRevLett.7.118.
- [3] B. I. Sturman and V. M. Fridkin, *The photovoltaic and photorefractive effects in noncentrosymmetric materials*, Gordon and Breach Science Publishers Philadelphia, Philadelphia (1992).
- [4] J. E. Spanier, V. M. Fridkin, A. M. Rappe, A. R. Akbashev, A. Polemi, Y. Qi, Z. Gu, S. M. Young, C. J. Hawley, D. Imbrenda, G. Xiao, A. L. Bennett-Jackson *et al.*, *Power conversion efficiency exceeding the shockley-queisser limit in a ferroelectric insulator*, Nature Photonics **10**(9), 611 (2016), doi:10.1038/nphoton.2016.143.

- [5] L. Wu, S. Patankar, T. Morimoto, N. L. Nair, E. Thewalt, A. Little, J. G. Analytis, J. E. Moore and J. Orenstein, *Giant anisotropic nonlinear optical response in transition metal monopnictide weyl semimetals*, Nature Physics **13**(4), 350 (2017), doi:10.1038/nphys3969.
- [6] S. Patankar, L. Wu, B. Lu, M. Rai, J. D. Tran, T. Morimoto, D. E. Parker, A. G. Grushin, N. L. Nair, J. G. Analytis, J. E. Moore, J. Orenstein *et al.*, *Resonance-enhanced optical nonlinearity in the weyl semimetal taas*, Phys. Rev. B **98**, 165113 (2018), doi:10.1103/PhysRevB.98.165113.
- [7] G. B. Osterhoudt, L. K. Diebel, M. J. Gray, X. Yang, J. Stanco, X. Huang, B. Shen, N. Ni, P. J. W. Moll, Y. Ran and K. S. Burch, *Colossal mid-infrared bulk photovoltaic effect in a type-i weyl semimetal*, Nature Materials **18**(5), 471 (2019), doi:10.1038/s41563-019-0297-4.
- [8] J. Ma, Q. Gu, Y. Liu, J. Lai, P. Yu, X. Zhuo, Z. Liu, J.-H. Chen, J. Feng and D. Sun, *Nonlinear photoresponse of type-ii weyl semimetals*, Nature Materials **18**(5), 476 (2019), doi:10.1038/s41563-019-0296-5.
- [9] Z. Ni, B. Xu, M.-Á. Sánchez-Martínez, Y. Zhang, K. Manna, C. Bernhard, J. W. F. Venderbos, F. de Juan, C. Felser, A. G. Grushin and L. Wu, *Linear and nonlinear optical responses in the chiral multifold semimetal rhsi*, npj Quantum Materials **5**(1), 96 (2020), doi:10.1038/s41535-020-00298-y.
- [10] T. Morimoto and N. Nagaosa, *Topological nature of nonlinear optical effects in solids*, Science Advances **2**(5), e1501524 (2016), doi:10.1126/sciadv.1501524, <https://www.science.org/doi/pdf/10.1126/sciadv.1501524>.
- [11] E. Luppi and V. Véniard, *A review of recent theoretical studies in nonlinear crystals: towards the design of new materials*, Semiconductor Science and Technology **31**(12), 123002 (2016), doi:10.1088/0268-1242/31/12/123002.
- [12] S. M. Young and A. M. Rappe, *First principles calculation of the shift current photovoltaic effect in ferroelectrics*, Phys. Rev. Lett. **109**, 116601 (2012), doi:10.1103/PhysRevLett.109.116601.
- [13] B. M. Fregoso, R. A. Muniz and J. E. Sipe, *Jerk current: A novel bulk photovoltaic effect*, Phys. Rev. Lett. **121**, 176604 (2018), doi:10.1103/PhysRevLett.121.176604.
- [14] B. M. Fregoso, *Bulk photovoltaic effects in the presence of a static electric field*, Phys. Rev. B **100**, 064301 (2019), doi:10.1103/PhysRevB.100.064301.
- [15] S. R. Panday, S. Barraza-Lopez, T. Rangel and B. M. Fregoso, *Injection current in ferroelectric group-iv monochalcogenide monolayers*, Phys. Rev. B **100**, 195305 (2019), doi:10.1103/PhysRevB.100.195305.
- [16] A. R. Puente-Uriona, S. S. Tsirkin, I. Souza and J. Ibañez Azpiroz, *Ab initio study of the nonlinear optical properties and dc photocurrent of the weyl semimetal tairte₄*, Phys. Rev. B **107**, 205204 (2023), doi:10.1103/PhysRevB.107.205204.
- [17] J. Sivianes, P. Garcia-Goiricelaya, D. Hernangómez-Pérez and J. Ibañez Azpiroz, *Surface-state engineering for generation of nonlinear charge and spin photocurrents*, Phys. Rev. Lett. **135**, 256201 (2025), doi:10.1103/h8rp-rtn8.
- [18] R. Martin, L. Reining and D. Ceperley, *Interacting Electrons*, Cambridge University Press, ISBN 9780521871501 (2016).

- [19] J. Deslippe, S. Louie and A. Rahman, *Ab initio theories of the structural, electronic, and optical properties of semiconductors: Bulk crystals to nanostructures*, In *Reference Module in Materials Science and Materials Engineering*. Elsevier, ISBN 978-0-12-803581-8, doi:<https://doi.org/10.1016/B978-0-12-803581-8.00764-5> (2016).
- [20] X. Liu, Q. Guo and J. Qiu, *Emerging low-dimensional materials for nonlinear optics and ultrafast photonics*, *Advanced Materials* **29**(14), 1605886 (2017), doi:<https://doi.org/10.1002/adma.201605886>, <https://advanced.onlinelibrary.wiley.com/doi/pdf/10.1002/adma.201605886>.
- [21] E. Runge and E. K. U. Gross, *Density-functional theory for time-dependent systems*, *Phys. Rev. Lett.* **52**, 997 (1984), doi:[10.1103/PhysRevLett.52.997](https://doi.org/10.1103/PhysRevLett.52.997).
- [22] E. K. U. Gross, J. F. Dobson and M. Petersilka, *Density functional theory of time-dependent phenomena*, pp. 81–172, Springer Berlin Heidelberg, Berlin, Heidelberg, ISBN 978-3-540-49946-6, doi:[10.1007/BFb0016643](https://doi.org/10.1007/BFb0016643) (1996).
- [23] H. Hübener, *Second-order response bethe-salpeter equation*, *Phys. Rev. A* **83**, 062122 (2011), doi:[10.1103/PhysRevA.83.062122](https://doi.org/10.1103/PhysRevA.83.062122).
- [24] J. Frenkel, *On the transformation of light into heat in solids. i*, *Phys. Rev.* **37**, 17 (1931), doi:[10.1103/PhysRev.37.17](https://doi.org/10.1103/PhysRev.37.17).
- [25] E. F. Gross, *Excitons and their motion in crystal lattices*, *Soviet Physics Uspekhi* **5**, 195 (1962), doi:[10.1070/PU1962v005n02ABEH003407](https://doi.org/10.1070/PU1962v005n02ABEH003407), [*Usp. Fiz. Nauk* **76**, 433-466 (1962)].
- [26] L. V. Keldysh and A. N. Kozlov, *Collective properties of excitons in semiconductors*, *Soviet Physics JETP* **27**, 521 (1968), doi:https://doi.org/10.1142/9789811279461_0011, [*Zh. Eksp. Teor. Fiz.* **54**,978-993 (1968)].
- [27] K. Kheng, R. T. Cox, M. Y. d' Aubigné, F. Bassani, K. Saminadayar and S. Tatarenko, *Observation of negatively charged excitons x^- in semiconductor quantum wells*, *Phys. Rev. Lett.* **71**, 1752 (1993), doi:[10.1103/PhysRevLett.71.1752](https://doi.org/10.1103/PhysRevLett.71.1752).
- [28] E. K. Chang, E. L. Shirley and Z. H. Levine, *Excitonic effects on optical second-harmonic polarizabilities of semiconductors*, *Phys. Rev. B* **65**, 035205 (2001), doi:[10.1103/PhysRevB.65.035205](https://doi.org/10.1103/PhysRevB.65.035205).
- [29] R. Leitsmann, W. G. Schmidt, P. H. Hahn and F. Bechstedt, *Second-harmonic polarizability including electron-hole attraction from band-structure theory*, *Phys. Rev. B* **71**, 195209 (2005), doi:[10.1103/PhysRevB.71.195209](https://doi.org/10.1103/PhysRevB.71.195209).
- [30] M. Grüning and C. Attaccalite, *Second harmonic generation in h-bn and mos₂ monolayers: Role of electron-hole interaction*, *Phys. Rev. B* **89**, 081102 (2014), doi:[10.1103/PhysRevB.89.081102](https://doi.org/10.1103/PhysRevB.89.081102).
- [31] M. Grüning and C. Attaccalite, *Erratum: Second harmonic generation in h-bn and mos₂ monolayers: Role of electron-hole interaction [phys. rev. b 89, 081102(r) (2014)]*, *Phys. Rev. B* **90**, 199901 (2014), doi:[10.1103/PhysRevB.90.199901](https://doi.org/10.1103/PhysRevB.90.199901).
- [32] M. L. Trolle, G. Seifert and T. G. Pedersen, *Theory of excitonic second-harmonic generation in monolayer mos₂*, *Phys. Rev. B* **89**, 235410 (2014), doi:[10.1103/PhysRevB.89.235410](https://doi.org/10.1103/PhysRevB.89.235410).

- [33] T. G. Pedersen, *Intraband effects in excitonic second-harmonic generation*, Phys. Rev. B **92**, 235432 (2015), doi:10.1103/PhysRevB.92.235432.
- [34] A. Riefer and W. G. Schmidt, *Solving the bethe-salpeter equation for the second-harmonic generation in zn chalcogenides*, Phys. Rev. B **96**, 235206 (2017), doi:10.1103/PhysRevB.96.235206.
- [35] A. Taghizadeh and T. G. Pedersen, *Gauge invariance of excitonic linear and nonlinear optical response*, Phys. Rev. B **97**, 205432 (2018), doi:10.1103/PhysRevB.97.205432.
- [36] R. Fei, L. Z. Tan and A. M. Rappe, *Shift-current bulk photovoltaic effect influenced by quasiparticle and exciton*, Phys. Rev. B **101**, 045104 (2020), doi:10.1103/PhysRevB.101.045104.
- [37] S. Konabe, *Exciton effect on shift current in single-walled boron-nitride nanotubes*, Phys. Rev. B **103**, 075402 (2021), doi:10.1103/PhysRevB.103.075402.
- [38] Z. Dai and A. M. Rappe, *First-principles calculation of ballistic current from electron-hole interaction*, Phys. Rev. B **104**, 235203 (2021), doi:10.1103/PhysRevB.104.235203.
- [39] Y. Chan, D. Y. Qiu, F. H. d. Jornada and S. G. Louie, *Giant exciton-enhanced shift currents and direct current conduction with subbandgap photo excitations produced by many-electron interactions*, Proceedings of the National Academy of Sciences **118** (2021), doi:10.1073/pnas.1906938118.
- [40] Y.-S. Huang, Y.-H. Chan and G.-Y. Guo, *Large shift currents via in-gap and charge-neutral excitons in a monolayer and nanotubes of bn*, Phys. Rev. B **108**, 075413 (2023), doi:10.1103/PhysRevB.108.075413.
- [41] J. Ruan, Y.-H. Chan and S. G. Louie, *Exciton enhanced nonlinear optical responses in monolayer h-bn and mos2: Insight from first-principles exciton-state coupling formalism and calculations*, Nano Letters **24**(49), 15533 (2024), doi:10.1021/acs.nanolett.4c03434, PMID: 39556702, <https://doi.org/10.1021/acs.nanolett.4c03434>.
- [42] J. J. Esteve-Paredes, M. A. García-Blázquez, A. J. Uría-Álvarez, M. Camarasa-Gómez and J. J. Palacios, *Excitons in nonlinear optical responses: shift current in mos2 and ges monolayers*, npj Computational Materials **11**(1), 13 (2025), doi:10.1038/s41524-024-01504-2.
- [43] H. Hübener, E. Luppi and V. Vénard, *Ab initio calculation of second harmonic generation in solids*, physica status solidi (b) **247**(8), 1984 (2010), doi:<https://doi.org/10.1002/pssb.200983954>, <https://onlinelibrary.wiley.com/doi/pdf/10.1002/pssb.200983954>.
- [44] E. Luppi, H. Hübener and V. Vénard, *Communications: Ab initio second-order nonlinear optics in solids*, The Journal of Chemical Physics **132**(24), 241104 (2010), doi:10.1063/1.3457671, https://pubs.aip.org/aip/jcp/article-pdf/doi/10.1063/1.3457671/16122687/241104_1_online.pdf.
- [45] E. Luppi, H. Hübener and V. Vénard, *Ab initio second-order nonlinear optics in solids: Second-harmonic generation spectroscopy from time-dependent density-functional theory*, Phys. Rev. B **82**, 235201 (2010), doi:10.1103/PhysRevB.82.235201.

- [46] H. Hübener, E. Luppi and V. Véniard, *Ab initio calculation of many-body effects on the second-harmonic generation spectra of hexagonal sic polytypes*, Phys. Rev. B **83**, 115205 (2011), doi:10.1103/PhysRevB.83.115205.
- [47] N. Gauriot, V. Véniard and E. Luppi, *Long-range corrected exchange-correlation kernels to describe excitons in second-harmonic generation*, The Journal of Chemical Physics **151**(23), 234111 (2019), doi:10.1063/1.5126501, https://pubs.aip.org/aip/jcp/article-pdf/doi/10.1063/1.5126501/15567310/234111_1_online.pdf.
- [48] P. Garcia-Goiricelaya, J. Krishna and J. Ibañez Azpiroz, *Including many-body effects into the wannier-interpolated quadratic photoresponse tensor*, Phys. Rev. B **107**, 205101 (2023), doi:10.1103/PhysRevB.107.205101.
- [49] A. Ramasubramaniam, *Large excitonic effects in monolayers of molybdenum and tungsten dichalcogenides*, Phys. Rev. B **86**, 115409 (2012), doi:10.1103/PhysRevB.86.115409.
- [50] A. Molina-Sánchez, D. Sangalli, K. Hummer, A. Marini and L. Wirtz, *Effect of spin-orbit interaction on the optical spectra of single-layer, double-layer, and bulk mos_2* , Phys. Rev. B **88**, 045412 (2013), doi:10.1103/PhysRevB.88.045412.
- [51] D. Y. Qiu, F. H. da Jornada and S. G. Louie, *Optical spectrum of mos_2 : Many-body effects and diversity of exciton states*, Phys. Rev. Lett. **111**, 216805 (2013), doi:10.1103/PhysRevLett.111.216805.
- [52] D. Y. Qiu, F. H. da Jornada and S. G. Louie, *Screening and many-body effects in two-dimensional crystals: Monolayer mos_2* , Phys. Rev. B **93**, 235435 (2016), doi:10.1103/PhysRevB.93.235435.
- [53] F. A. Rasmussen, P. S. Schmidt, K. T. Winther and K. S. Thygesen, *Efficient many-body calculations for two-dimensional materials using exact limits for the screened potential: Band gaps of mos_2 , $h\text{-bn}$, and phosphorene*, Phys. Rev. B **94**, 155406 (2016), doi:10.1103/PhysRevB.94.155406.
- [54] J. S. Ross, S. Wu, H. Yu, N. J. Ghimire, A. M. Jones, G. Aivazian, J. Yan, D. G. Mandrus, D. Xiao, W. Yao and X. Xu, *Electrical control of neutral and charged excitons in a monolayer semiconductor*, Nature Communications **4**(1), 1474 (2013), doi:10.1038/ncomms2498.
- [55] K. F. Mak, K. He, C. Lee, G. H. Lee, J. Hone, T. F. Heinz and J. Shan, *Tightly bound trions in monolayer mos_2* , Nature Materials **12**(3), 207 (2013), doi:10.1038/nmat3505.
- [56] L. M. Malard, T. V. Alencar, A. P. M. Barboza, K. F. Mak and A. M. de Paula, *Observation of intense second harmonic generation from mos_2 atomic crystals*, Phys. Rev. B **87**, 201401 (2013), doi:10.1103/PhysRevB.87.201401.
- [57] Y. J. Zhang, T. Ideue, M. Onga, F. Qin, R. Suzuki, A. Zak, R. Tenne, J. H. Smet and Y. Iwasa, *Enhanced intrinsic photovoltaic effect in tungsten disulfide nanotubes*, Nature **570**(7761), 349 (2019), doi:10.1038/s41586-019-1303-3.
- [58] J. Krishna, P. Garcia-Goiricelaya, F. de Juan and J. Ibañez Azpiroz, *Understanding the large shift photocurrent of ws_2 nanotubes: A comparative analysis with monolayers*, Phys. Rev. B **108**, 165418 (2023), doi:10.1103/PhysRevB.108.165418.

- [59] G. Vignale and W. Kohn, *Current-dependent exchange-correlation potential for dynamical linear response theory*, Phys. Rev. Lett. **77**, 2037 (1996), doi:10.1103/PhysRevLett.77.2037.
- [60] G. Vignale, C. A. Ullrich and S. Conti, *Time-dependent density functional theory beyond the adiabatic local density approximation*, Phys. Rev. Lett. **79**, 4878 (1997), doi:10.1103/PhysRevLett.79.4878.
- [61] P. Hohenberg and W. Kohn, *Inhomogeneous electron gas*, Phys. Rev. **136**, B864 (1964), doi:10.1103/PhysRev.136.B864.
- [62] W. Kohn and L. J. Sham, *Self-consistent equations including exchange and correlation effects*, Phys. Rev. **140**, A1133 (1965), doi:10.1103/PhysRev.140.A1133.
- [63] J. P. Perdew and A. Zunger, *Self-interaction correction to density-functional approximations for many-electron systems*, Phys. Rev. B **23**, 5048 (1981), doi:10.1103/PhysRevB.23.5048.
- [64] P. Giannozzi, S. Baroni, N. Bonini, M. Calandra, R. Car, C. Cavazzoni, D. Ceresoli, G. L. Chiarotti, M. Cococcioni, I. Dabo, A. D. Corso, S. de Gironcoli *et al.*, *Quantum espresso: a modular and open-source software project for quantum simulations of materials*, Journal of Physics: Condensed Matter **21**(39), 395502 (2009), doi:10.1088/0953-8984/21/39/395502.
- [65] P. Giannozzi, O. Andreussi, T. Brumme, O. Bunau, M. B. Nardelli, M. Calandra, R. Car, C. Cavazzoni, D. Ceresoli, M. Cococcioni, N. Colonna, I. Carnimeo *et al.*, *Advanced capabilities for materials modelling with quantum espresso*, Journal of Physics: Condensed Matter **29**(46), 465901 (2017), doi:10.1088/1361-648X/aa8f79.
- [66] P. Giannozzi, O. Baseggio, P. Bonfà, D. Brunato, R. Car, I. Carnimeo, C. Cavazzoni, S. de Gironcoli, P. Delugas, F. Ferrari Ruffino, A. Ferretti, N. Marzari *et al.*, *Quantum ESPRESSO toward the exascale*, The Journal of Chemical Physics **152**(15), 154105 (2020), doi:10.1063/5.0005082.
- [67] L. Kleinman, *Relativistic norm-conserving pseudopotential*, Phys. Rev. B **21**, 2630 (1980), doi:10.1103/PhysRevB.21.2630.
- [68] D. R. Hamann, *Generalized norm-conserving pseudopotentials*, Phys. Rev. B **40**, 2980 (1989), doi:10.1103/PhysRevB.40.2980.
- [69] D. R. Hamann, *Optimized norm-conserving vanderbilt pseudopotentials*, Phys. Rev. B **88**, 085117 (2013), doi:10.1103/PhysRevB.88.085117.
- [70] M. Schlipf and F. Gygi, *Optimization algorithm for the generation of oncv pseudopotentials*, Computer Physics Communications **196**, 36 (2015), doi:https://doi.org/10.1016/j.cpc.2015.05.011.
- [71] P. Scherpelz, M. Govoni, I. Hamada and G. Galli, *Implementation and validation of fully relativistic gw calculations: Spin-orbit coupling in molecules, nanocrystals, and solids*, Journal of Chemical Theory and Computation **12**(8), 3523 (2016), doi:10.1021/acs.jctc.6b00114, PMID: 27331614.
- [72] A. Molina-Sánchez, K. Hummer and L. Wirtz, *Vibrational and optical properties of mos2: From monolayer to bulk*, Surface Science Reports **70**(4), 554 (2015), doi:https://doi.org/10.1016/j.surfrep.2015.10.001.

- [73] P. A. Young, *Lattice parameter measurements on molybdenum disulphide*, Journal of Physics D: Applied Physics **1**(7), 936 (1968), doi:10.1088/0022-3727/1/7/416.
- [74] T. Sohler, M. Calandra and F. Mauri, *Density functional perturbation theory for gated two-dimensional heterostructures: Theoretical developments and application to flexural phonons in graphene*, Phys. Rev. B **96**, 075448 (2017), doi:10.1103/PhysRevB.96.075448.
- [75] A. Molina-Sánchez and L. Wirtz, *Phonons in single-layer and few-layer mos_2 and ws_2* , Phys. Rev. B **84**, 155413 (2011), doi:10.1103/PhysRevB.84.155413.
- [76] P. Garcia-Goiricelaya, J. Lafuente-Bartolome, I. G. Gurtubay and A. Eiguren, *Emergence of large nonadiabatic effects induced by the electron-phonon interaction on the complex vibrational quasiparticle spectrum of doped monolayer mos_2* , Phys. Rev. B **101**, 054304 (2020), doi:10.1103/PhysRevB.101.054304.
- [77] L. Hedin, *New method for calculating the one-particle green's function with application to the electron-gas problem*, Phys. Rev. **139**, A796 (1965), doi:10.1103/PhysRev.139.A796.
- [78] L. Hedin and S. Lundqvist, *Effects of electron-electron and electron-phonon interactions on the one-electron states of solids*, vol. 23 of *Solid State Physics*, pp. 1–181. Academic Press, doi:https://doi.org/10.1016/S0081-1947(08)60615-3 (1970).
- [79] E. E. Salpeter and H. A. Bethe, *A relativistic equation for bound-state problems*, Phys. Rev. **84**, 1232 (1951), doi:10.1103/PhysRev.84.1232.
- [80] A. Marini, C. Hogan, M. Grüning and D. Varsano, *yambo: An ab initio tool for excited state calculations*, Computer Physics Communications **180**(8), 1392 (2009), doi:https://doi.org/10.1016/j.cpc.2009.02.003.
- [81] D. Sangalli, A. Ferretti, H. Miranda, C. Attaccalite, I. Marri, E. Cannuccia, P. Melo, M. Marsili, F. Paleari, A. Marrazzo, G. Prandini, P. Bonfà *et al.*, *Many-body perturbation theory calculations using the yambo code*, Journal of Physics: Condensed Matter **31**(32), 325902 (2019), doi:10.1088/1361-648X/ab15d0.
- [82] B. I. Lundqvist, *Single-particle spectrum of the degenerate electron gas*, Physik der kondensierten Materie **6**(3), 193 (1967), doi:10.1007/BF02422716.
- [83] B. I. Lundqvist, *Single-particle spectrum of the degenerate electron gas*, Physik der kondensierten Materie **6**(3), 206 (1967), doi:10.1007/BF02422717.
- [84] A. W. Overhauser, *Simplified theory of electron correlations in metals*, Phys. Rev. B **3**, 1888 (1971), doi:10.1103/PhysRevB.3.1888.
- [85] F. Bruneval and X. Gonze, *Accurate gw self-energies in a plane-wave basis using only a few empty states: Towards large systems*, Phys. Rev. B **78**, 085125 (2008), doi:10.1103/PhysRevB.78.085125.
- [86] A. Guandalini, P. D'Amico, A. Ferretti and D. Varsano, *Efficient gw calculations in two dimensional materials through a stochastic integration of the screened potential*, npj Computational Materials **9**(1), 44 (2023), doi:10.1038/s41524-023-00989-7.
- [87] R. Haydock, *The recursive solution of the schrodinger equation*, vol. 35 of *Solid State Physics*, pp. 215–294. Academic Press, doi:https://doi.org/10.1016/S0081-1947(08)60505-6 (1980).

- [88] J. E. Sipe and E. Ghahramani, *Nonlinear optical response of semiconductors in the independent-particle approximation*, Phys. Rev. B **48**, 11705 (1993), doi:10.1103/PhysRevB.48.11705.
- [89] C. Aversa and J. E. Sipe, *Nonlinear optical susceptibilities of semiconductors: Results with a length-gauge analysis*, Phys. Rev. B **52**, 14636 (1995), doi:10.1103/PhysRevB.52.14636.
- [90] J. E. Sipe and A. I. Shkrebtii, *Second-order optical response in semiconductors*, Phys. Rev. B **61**, 5337 (2000), doi:10.1103/PhysRevB.61.5337.
- [91] J. Ibañez Azpiroz, S. S. Tsirkin and I. Souza, *Ab initio calculation of the shift photocurrent by wannier interpolation*, Phys. Rev. B **97**, 245143 (2018), doi:10.1103/PhysRevB.97.245143.
- [92] G. Pizzi, V. Vitale, R. Arita, S. Blügel, F. Freimuth, G. Géranton, M. Gibertini, D. Gresch, C. Johnson, T. Koretsune, J. Ibañez-Azpiroz, H. Lee *et al.*, *Wannier90 as a community code: new features and applications*, Journal of Physics: Condensed Matter **32**(16), 165902 (2020), doi:10.1088/1361-648x/ab51ff.
- [93] Y.-h. Chan, J. B. Haber, M. H. Naik, J. B. Neaton, D. Y. Qiu, F. H. da Jornada and S. G. Louie, *Exciton lifetime and optical line width profile via exciton-phonon interactions: Theory and first-principles calculations for monolayer mos₂*, Nano Letters **23**(9), 3971 (2023), doi:10.1021/acs.nanolett.3c00732, PMID: 37071728, <https://doi.org/10.1021/acs.nanolett.3c00732>.
- [94] A. Molina-Sánchez, G. Catarina, D. Sangalli and J. Fernández-Rossier, *Magneto-optical response of chromium trihalide monolayers: chemical trends*, J. Mater. Chem. C **8**, 8856 (2020), doi:10.1039/D0TC01322F.
- [95] G. A. Ermolaev, Y. V. Stebunov, A. A. Vyshnevyy, D. E. Tatarkin, D. I. Yakubovsky, S. M. Novikov, D. G. Baranov, T. Shegai, A. Y. Nikitin, A. V. Arsenin and V. S. Volkov, *Broadband optical properties of monolayer and bulk mos₂*, npj 2D Materials and Applications **4**(1), 21 (2020), doi:10.1038/s41699-020-0155-x.
- [96] L. Reining, V. Olevano, A. Rubio and G. Onida, *Excitonic effects in solids described by time-dependent density-functional theory*, Phys. Rev. Lett. **88**, 066404 (2002), doi:10.1103/PhysRevLett.88.066404.
- [97] G. Onida, L. Reining and A. Rubio, *Electronic excitations: density-functional versus many-body green's-function approaches*, Rev. Mod. Phys. **74**, 601 (2002), doi:10.1103/RevModPhys.74.601.
- [98] F. Sottile, K. Karlsson, L. Reining and F. Aryasetiawan, *Macroscopic and microscopic components of exchange-correlation interactions*, Phys. Rev. B **68**, 205112 (2003), doi:10.1103/PhysRevB.68.205112.
- [99] S. Botti, F. Sottile, N. Vast, V. Olevano, L. Reining, H.-C. Weissker, A. Rubio, G. Onida, R. Del Sole and R. W. Godby, *Long-range contribution to the exchange-correlation kernel of time-dependent density functional theory*, Phys. Rev. B **69**, 155112 (2004), doi:10.1103/PhysRevB.69.155112.
- [100] Y.-M. Byun and C. A. Ullrich, *Assessment of long-range-corrected exchange-correlation kernels for solids: Accurate exciton binding energies via an empirically scaled bootstrap kernel*, Phys. Rev. B **95**, 205136 (2017), doi:10.1103/PhysRevB.95.205136.

- [101] S. Sharma, J. K. Dewhurst, A. Sanna and E. K. U. Gross, *Bootstrap approximation for the exchange-correlation kernel of time-dependent density-functional theory*, Phys. Rev. Lett. **107**, 186401 (2011), doi:10.1103/PhysRevLett.107.186401.
- [102] V. U. Nazarov and G. Vignale, *Optics of semiconductors from meta-generalized-gradient-approximation-based time-dependent density-functional theory*, Phys. Rev. Lett. **107**, 216402 (2011), doi:10.1103/PhysRevLett.107.216402.
- [103] P. E. Trevisanutto, A. Terentjevs, L. A. Constantin, V. Olevano and F. D. Sala, *Optical spectra of solids obtained by time-dependent density functional theory with the jellium-with-gap-model exchange-correlation kernel*, Phys. Rev. B **87**, 205143 (2013), doi:10.1103/PhysRevB.87.205143.
- [104] S. Rigamonti, S. Botti, V. Veniard, C. Draxl, L. Reining and F. Sottile, *Estimating excitonic effects in the absorption spectra of solids: Problems and insight from a guided iteration scheme*, Phys. Rev. Lett. **114**, 146402 (2015), doi:10.1103/PhysRevLett.114.146402.
- [105] J. A. Berger, *Fully parameter-free calculation of optical spectra for insulators, semiconductors, and metals from a simple polarization functional*, Phys. Rev. Lett. **115**, 137402 (2015), doi:10.1103/PhysRevLett.115.137402.
- [106] S. Sharma, J. K. Dewhurst, A. Sanna and E. K. U. Gross, *Comment on “estimating excitonic effects in the absorption spectra of solids: Problems and insight from a guided iteration scheme”*, Phys. Rev. Lett. **117**, 159701 (2016), doi:10.1103/PhysRevLett.117.159701.
- [107] S. Rigamonti, S. Botti, V. Veniard, C. Draxl, L. Reining and F. Sottile, *Rigamonti et al. reply*, Phys. Rev. Lett. **117**, 159702 (2016), doi:10.1103/PhysRevLett.117.159702.
- [108] R. Del Sole, G. Adragna, V. Olevano and L. Reining, *Long-range behavior and frequency dependence of exchange-correlation kernels in solids*, Phys. Rev. B **67**, 045207 (2003), doi:10.1103/PhysRevB.67.045207.
- [109] S. Botti, A. Fourreau, F. m. c. Nguyen, Y.-O. Renault, F. Sottile and L. Reining, *Energy dependence of the exchange-correlation kernel of time-dependent density functional theory: A simple model for solids*, Phys. Rev. B **72**, 125203 (2005), doi:10.1103/PhysRevB.72.125203.
- [110] D. R. Gulevich, Y. V. Zhumagulov, V. K. Kozin and I. V. Tokatly, *Excitonic effects in time-dependent density functional theory from zeros of the density response*, Phys. Rev. B **107**, 165118 (2023), doi:10.1103/PhysRevB.107.165118.